Definitive Support by Transmission Electron Microscopy, Electron Diffraction, and Electron Density Maps for the Formation of a BCC Lattice from Poly{*N*-[3,4,5-tris(*n*-dodecan-l-yloxy)benzoyl]ethyleneimine}

Hu Duan,[b] Steven D. Hudson,[b] Goran Ungar,[c] Marian N. Holerca,[a] and Virgil Percec[a]*

Abstract: Transmission electron microscopy (TEM), electron diffraction (ED), and electron density maps (EDM) experiments were carried out on a poly{*N*-[3,4,5-tris(*n*-dodecan-l-yloxy)benzoyl]-ethyleneimine} {**poly[(3,4,5)12G1-Oxz]**} with a degree of polymerization (DP) of 20. All experiments confirmed the thermotropic body-centered cubic (BCC) $Im\bar{3}m$ lattice suggested previously by X-ray diffraction (XRD) experiments. The unit cell parameter determined by ED at 23 °C is $a = 42.4$ Å, in good agreement with XRD results which show $a = 42.6$ Å after quenching from 70 °C. EDM of the XRD results confirm that the supramolecular minidendrimer obtained from **poly[(3,4,5)12G1-Oxz]** adopts a spherical "inverse micellar-like" structure, with the polyethyleneimine backbone and the aromatic groups microsegregated and concentrated in the corners and in the center of the cubic unit cell. A space-filling continuum is realized by the *n*-alkyl groups that radiate out of the aromatic core of the spherical dendrimer. This manuscript is only the second example of complete structural analysis of a lattice generated from supramolecular objects and complements the previous example reported from our laboratory on the $Pm\bar{3}n$ lattice.

Keywords: dendrimers · electron density · electron diffraction · electron microscopy · supramolecular chemistry

Introduction

Our laboratory has elaborated strategies for the design and synthesis of monodendritic and minidendritic building blocks that self-assemble in bulk into supramolecular dendrimers. Upon functionalization with suitable polymerizable groups followed by polymerization, the same monodendrons generate macromolecular dendrimers. Both the supramolecular and the macromolecular dendrimers exhibit shapes that have the perfection to self-organize and co-organize in two-dimensional (2-D) and three-dimensional (3-D) lattices and superlattices (Scheme 1). So far, we have reported the 2-D *p6mm* hexagonal columnar lattices[1a,e, 2] self-organized from cylindrical supramolecular and macromolecular dendrimers and the hexagonal columnar superlattices[3] co-organized from mixtures of 3-cylindrical bundle supramolecular minidendrimers with cylindrical supramolecular minidendrimers. We have also reported the synthesis of spherical molecular, supramolecular and macromolecular dendrimers that are able to self-organize into three-dimensional (3-D) $Pm\bar{3}n$[4] and $Im\bar{3}m$[5] cubic lattices.

The rational approach to the design of these building blocks involves the determination of the lattice in which the molecular, supramolecular and macromolecular dendrimers are self-organized followed by the retrostructural analysis of this lattice (Scheme 1). In the first step of this process, a combination of differential scanning calorimetry (DSC) and thermal optical polarized microscopy (TOPM) is used to identify a lattice.[1a,e, 2–5] These experiments produce a qualitative estimation of the nature of the bulk phase. Subsequently, X-ray diffraction experiments (XRD) performed on single crystal or single crystal liquid crystal specimens are used to determine the lattice symmetry.[1a,e,n, 2–5] A combination of electron density maps (EDM), transmission electron microscopy (TEM), and electron diffraction experiments (ED) is used to confirm the symmetry of the lattice and to determine the shape of the objects that forms the lattice.[1d, 4, 6] During this structural analysis process, various modes of self-assembly of the monodendritic building blocks into supramolecular

[a] Prof. V. Percec, Dr. M. N. Holerca
Roy&Diana Vagelos Laboratories
Department of Chemistry and Laboratory
for Research on the Structure of Matter
University of Pennsylvania, Philadelphia, PA 19104-6323 (USA)
Fax: 215-573-7888
E-mail: percec@sas.upenn.edu

[b] Prof. H. Duan, Prof. S. D. Hudson
Department of Macromolecular Science
Case Western Reserve University, Cleveland, OH 44106 (USA)

[c] Dr. G. Ungar
Department of Engineering Materials
and Center for Molecular Materials
University of Sheffield, Sheffield S1 3JD (UK)

0947-6539/01/0719-4134 $ 17.50+.50/0

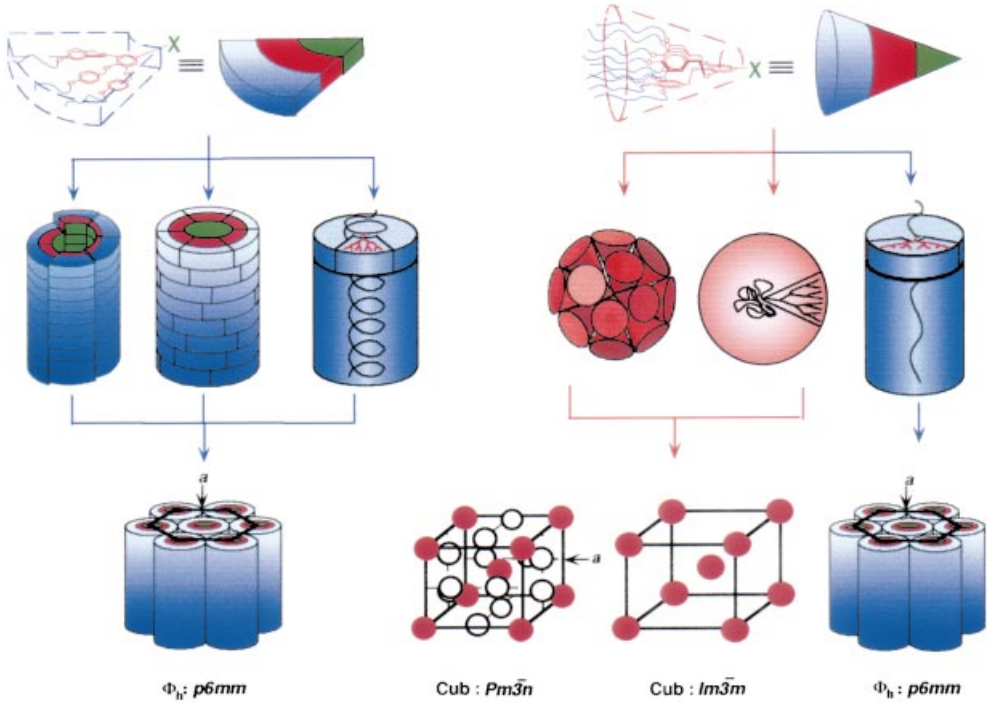

Scheme 1. Rational design of libraries of quasi-equivalent dendritic building blocks through retrostructural analysis of the lattices self-organized from their supramolecular and macromolecular dendrimers. (a = lattice dimension).

objects of different shapes and their subsequent self-organization in lattices is screened by EDM. After the shape of these supramolecular and macromolecular objects in the bulk phase is determined by these methods, scanning force microscopy (SFM) is used to visualize them in a lattice or as individual molecules on a surface.[2i,j] Finally, the retrostructural analysis of lattices generated from supramolecular dendrimers of known shapes by using the lattice dimensions, the mode of self-assembly of the monodendrons and the density data provides access to the shape, size, and number of monodendritic building blocks that form the supramolecular or macromolecular dendrimer.[1a–e, 4, 7]

Recently, we have discovered that poly{*N*-[3,4,5-tris-(*n*-dodecan-l-yloxy)benzoyl]ethyleneimine} {**poly[(3,4,5)12G1-Oxz]**} with a degree of polymerization DP = 20 forms most probably an "inverse micellar"- or "water-in-oil"-like (similar to the lyotropic type I_{II}) thermotropic body-centered cubic (BCC) liquid crystal (LC) phase. Fiber X-ray diffraction (XRD) experiments showed that the extinction symbol of this phase is *I*—and the most probable space group of the lattice was considered to be $Im\bar{3}m$ (Q^{229}). The unit cell parameter is $a = 42.6$ Å.

Phase separated cubic morphologies were observed previously in the field of block-copolymers.[8] A "micellar" type $Im\bar{3}m$ phase was first shown by electron microscopy in a triblock copolymer[9] and later by neutron scattering in a diblock compound.[10] Nevertheless, the "micellar" type phase from block copolymers does not belong to the $Im\bar{3}m$ "inverse micellar-like" classification, as in the case of the LC lattice formed by **poly[(3,4,5)12G1-Oxz]**.[5] This lattice is encountered in many other examples of supramolecular and macromolecular dendrimers synthesized in our laboratory and its retrostructural analysis will be used in the determination of the shape of their corresponding monodendrons. Therefore, a definitive elucidation of the lattice space group and the mode of self-assembly of the monodendrons in the corresponding supramolecular dendrimers is necessary. The goal of this publication is to provide the definitive demonstration of this lattice space group, of the shape of the objects that create the lattice and of the mode of self-assembly of the repeat units of **poly[(3,4,5)12G1-Oxz]** by a combination of TEM, ED and EDM.

Results and Discussion

The DSC trace of **poly[(3,4,5)12G1-Oxz]** (DP = 20) recorded at 10 °C min^{-1} (Figure 1) shows two endothermic transitions on heating: one at −12 °C ($\Delta H = 19.5$ J g^{-1}), into the thermotropic LC phase and another at 131 °C ($\Delta H = 1.7$ J g^{-1}), into the isotropic liquid. On cooling the reverse sequence of transitions occurs, with a small hysteresis (exothermic peaks at 122 °C and −16 °C).

TOPM was used to assess qualitatively the structure and properties of **poly[(3,4,5)12G1-Oxz]** at various temperatures. At room temperature, no birefringence was detected under crossed polarizers in the thermotropic LC phase. The material is optically isotropic. Upon heating, the material shows no change in terms of birefringence. Using bright field observation, a significant reduction in viscosity was observed at 125 °C, that is approximately the transition temperature measured by DSC (the peak endotherm temperature equals 131 °C at a heating rate of 10 °C min^{-1}). The optical isotropy and relatively high viscosity indicate that the phase at $T < 125$ °C is cubic as shown by XRD.[5]

  0947-6539/01/0719-4135 $ 17.50+.50/0

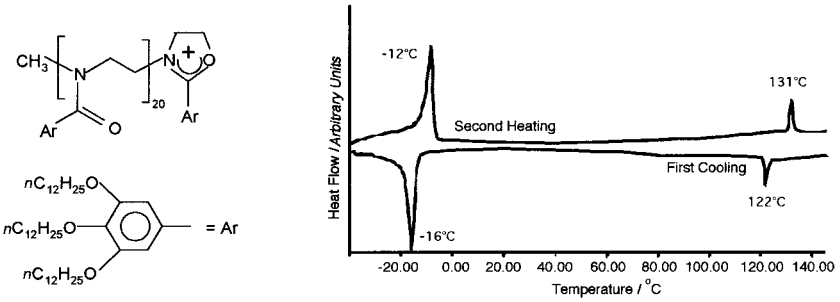

Figure 1. The molecular repeating structure (left side) and the second heating and first cooling DSC scans ($10\,^{\circ}C\,min^{-1}$) of **poly[(3,4,5)12G1-Oxz]** with DP = 20.

Previous characterization by XRD, indicated diffraction arcs arranged in rings with relative reciprocal spacing equal to $1:\sqrt{2}:\sqrt{3}:\sqrt{4}:\sqrt{5}$ etc., consistent with a cubic lattice. The absence of {421} reflections indicated that the extinction symbol is *I*, which indicates a body centered symmetry. Several centrosymmetric and non-centrosymmetric space groups are possible: $Im\bar{3}m$ (#229), $I\bar{4}3m$ (#217), $I432$ (#211), $Im\bar{3}$ (#204), $I23$ (#197), and $I2_13$ (#199).

Samples with carbon encapsulation (see Experimental Section) were more suitable for TEM examination, because without the second layer, the material could redistribute during annealing, forming generally thicker films with a stepped morphology (i.e., with discrete thickness). The graded morphology is clearly shown by discrete color domains of the reflected light image (Figure 2). Since the color changes abruptly, it indicates that the thickness also changes abruptly. That is, the image is stepped or terraced. This happens during annealing in order to reduce surface energy. If the film thickness were to change more gradually, many higher-energy microscopic steps would exist. During annealing, these coalesce together to reduce the total energy associated with the steps. A schematic illustration of the low energy (110) steps is shown in Figure 2b.

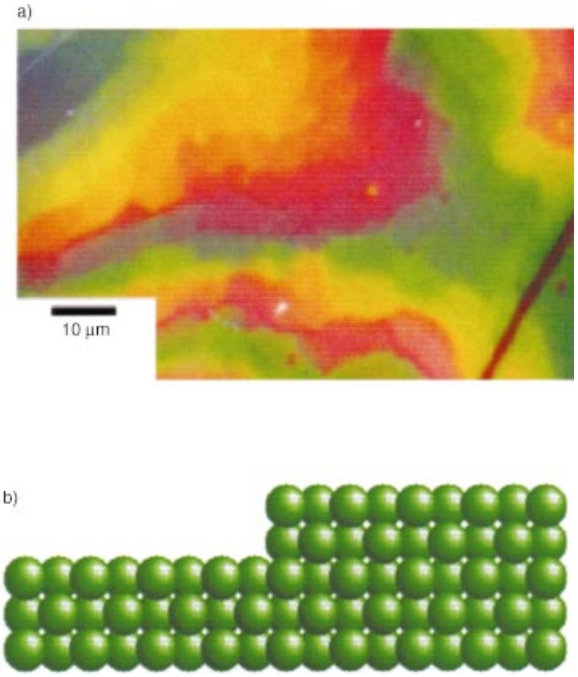

Figure 2. a) Reflection optical microscope image of stepped morphology of **poly[(3,4,5)12G1-Oxz]** with DP = 20 annealed on carbon coated mica. b) A schematic representation of the stepped morphology; (110) planes.

Figure 3 shows different zone-axis ED patterns of the cubic phase. Sharp diffraction spots were observed, and large grain size was further confirmed by translation of the specimen several micrometers before observing a change in the orientation of the crystallographic axes. The principal orientation of the structure was such that the (110) plane was in contact with the carbon substrate. Therefore, at normal beam incidence, the diffraction pattern has a two-fold symmetry (Figure 3b). By tilting the sample about the [002] axis by approximately 45°, a four-fold symmetry appeared (Figure 3a). Alternatively, if the sample is tilted from the normal beam incidence about the orthogonal [110] axis by approximately 35°, the hexagonal symmetric [111] zone axis pattern appears.[3a] From Figure 3a the four-fold rotation symmetry is clear. Therefore, the point symmetry of the reciprocal space (i.e., Laue class) is $m\bar{3}m$. This assignment quickly eliminates three of the possibilities ($Im\bar{3}$ (#204), $I23$ (#197) and $I2_13$ (#199)) and leaves only $Im\bar{3}m$ (#229), $I\bar{4}3m$ (#217), $I432$ (#211) if we consider the two-, three- and four-fold symmetry in the diffraction pattern shown in Figure 3b, c and a, respectively (see Table 1).

By quantitative analysis of the diffraction spot intensity (e.g., Figure 4), we found that the intensity of the 110 reflections is 30 to 100 times greater than that for the other reflection planes. In total, four unique reflections were observed: (110), (200), (211), and (220). Their respective relative peak intensities were approximately 1, 0.03, 0.01, and 0.01. When comparing to the XRD data,[5] one must multiply these intensities by the relative multiplicity of each respective reflection. As such, the relative intensities are approximately 1, 0.015, 0.02, and 0.01. This result agrees again well with the results from the XRD diffraction spot intensities.

TEM images were also obtained from each of the zone axes, that is [100], [011], and [111] (Figure 3). The Fourier transform power spectra of these images reproduce the ED patterns from each zone. From analysis of the images and the ED patterns, the $d_{110} = 30.0$ Å and consequently, the unit cell parameter is determined as $a = \sqrt{2}d_{110}$, which is 42.4 Å. These results also agree with the experimental measurements of XRD[5] that were obtained at 23 °C showing $d_{110} = 30.3$ Å and $a = 42.6$ Å. The slight difference can be attributed to an analogous decrease of the column diameter with increasing temperature as observed previously[11] in such systems as a dual thinning effect: a) the increase of the *γ-gauche* conformers in the paraffine tails, equivalent to a lateral shrinkage; b) the building blocks are "shedding off", forming thinner columns, more stable thermodynamicaly.

Considering the following arguments, it is most likely that the space group is $Im\bar{3}m$. If the unit cell in each instance contained two micelles, the $Im\bar{3}m$ and $I432$ are quite different.

  0947-6539/01/0719-4136 $ 17.50+.50/0 *Chem. Eur. J.* **2001**, *7*, No. 19

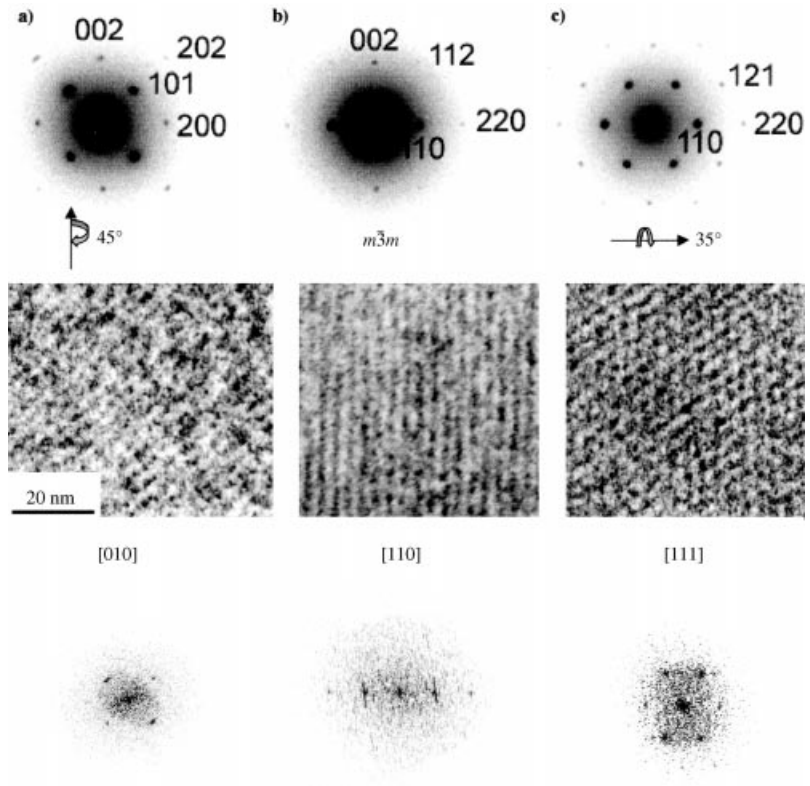

Figure 3. Electron diffraction patterns, TEM images, and Fourier transform power spectra of the TEM images of **poly[(3,4,5)12G1-Oxz]** DP = 20. The electron diffraction patterns correspond to the images below. a) [010] projection; b) [110] projection; c) [111] projection.

Table 1. Symmetry operation of five cubic point groups.

Schoenflies	International	Symmetry operation
T	23	$E\ 8C_3\ 3C_2$
T_h	$m\bar{3}$	$E\ 8C_3\ 3C_2\ I\ 8S_6\ 3\sigma_h$
O	432	$E\ 8C_3\ 3C_2\ 6C_2\ 6C_4$
T_d	$\bar{4}3m$	$E\ 8C_3\ 3C_2\ 6\sigma_d\ 6S_4$
O_h	$m\bar{3}m$	$E\ 8C_3\ 3C_2\ 6C_2\ 6C_4\ I\ 8S_6\ 3\sigma_h\ 6\sigma_d\ 6S_4$

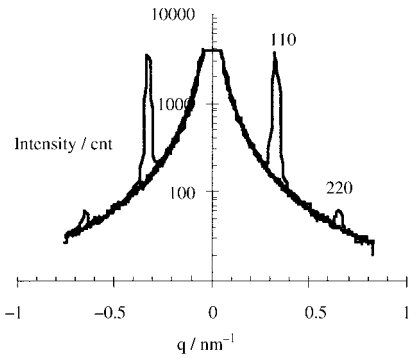

Figure 4. An intensity profile along the horizontal line through the center of the electron diffraction pattern recorded on a Fuji image plate, as shown in Figure 3a. The dark curve is Lorentzian fit to the background intensity that originates from inelastic scattering diffraction spots. Peak intensities reported in the text were determined after background substraction.

If the space group is $I432$, the micelles are chiral while the $Im\bar{3}m$ micelles have octahedral symmetry. The nature of the disorder in lattices generated from supramolecular objects favors molecule aggregation of highest symmetry (Figure 5). There will be no particular interaction or molecular force to cause the micelles to form asymmetric structures.

In order to obtain information on spatial organization of molecular sub-units and test the consistency of our model with the measured diffraction intensities, we proceeded to reconstruct the electron density distribution $\rho(x,y,z)$ using the intensities of the first four strongest XRD peaks listed in Table 2. Higher diffraction peaks are significantly weaker and their contribution to ρ was neglected. Fourier summation was performed using the amplitudes F_{hkl} in Table 2 and taking due account of $Im\bar{3}m$ symmetry. The procedure was similar to that described for the $Pm\bar{3}n$ phase.[4] Since the space group is centrosymmetric the structure factor is real and the phase problem reduces to the choice of sign in the summation. For $Im\bar{3}m$ both the amplitude and

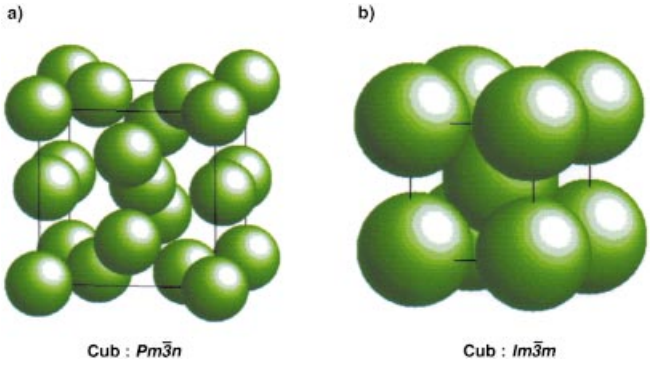

Figure 5. Schematic representation of spherical micellar-like objects in the $Pm\bar{3}n$ and $Im\bar{3}m$ lattices (only aromatic part is shown).

Table 2. Integrated X-ray powder diffraction intensities (I_{hkl}) and the corresponding structure factors F_{hkl} for the $Im\bar{3}m$ phase in **poly-[(3,4,5)12G1-Oxz]** (arbitrary units).

hkl	I_{hkl}	F_{hkl}
110	100	100
200	1.4	23
211	2.2	18
220	1.1	21

the phase are invariant to permutation of indices. Out of the $2^4 = 16$ possible phase combinations, eight are related to the other eight through $\rho'(x,y,z) = -\rho(x,y,z)$. In order to facilitate a physically plausible choice electron density histograms were calculated for each phase combination by

sampling ρ (x,y,z) at 50^3 points in a unit cell. Eight histograms (volume fraction versus electron density) are shown in Figure 6, with the other eight being their mirror images.

It was established by molecular modeling that 22.5% of volume is occupied by the high electron density fraction of the molecule, that is backbone and the 3,4,5-trioxybenzyl residues. The remaining 77.5% is occupied by the low electron density *n*-dodecyl groups. Based on previous observations,[4] we assume that a microphase separation occurs between the aromatic and aliphatic moieties, we expect a large fraction of the volume represented by the aliphatic fraction to be of nearly constant low density, which should give rise to a narrow peak on the low-density side of the histogram. In an ideal two-phase structure with constant ρ within each sub-phase the histogram would consist of only two sharp peaks with areas reflecting the volume ratio of the sub-phases. Although none of the histograms in Figure 6 complies with this idealized situation, the histogram with all phase angles equal to zero

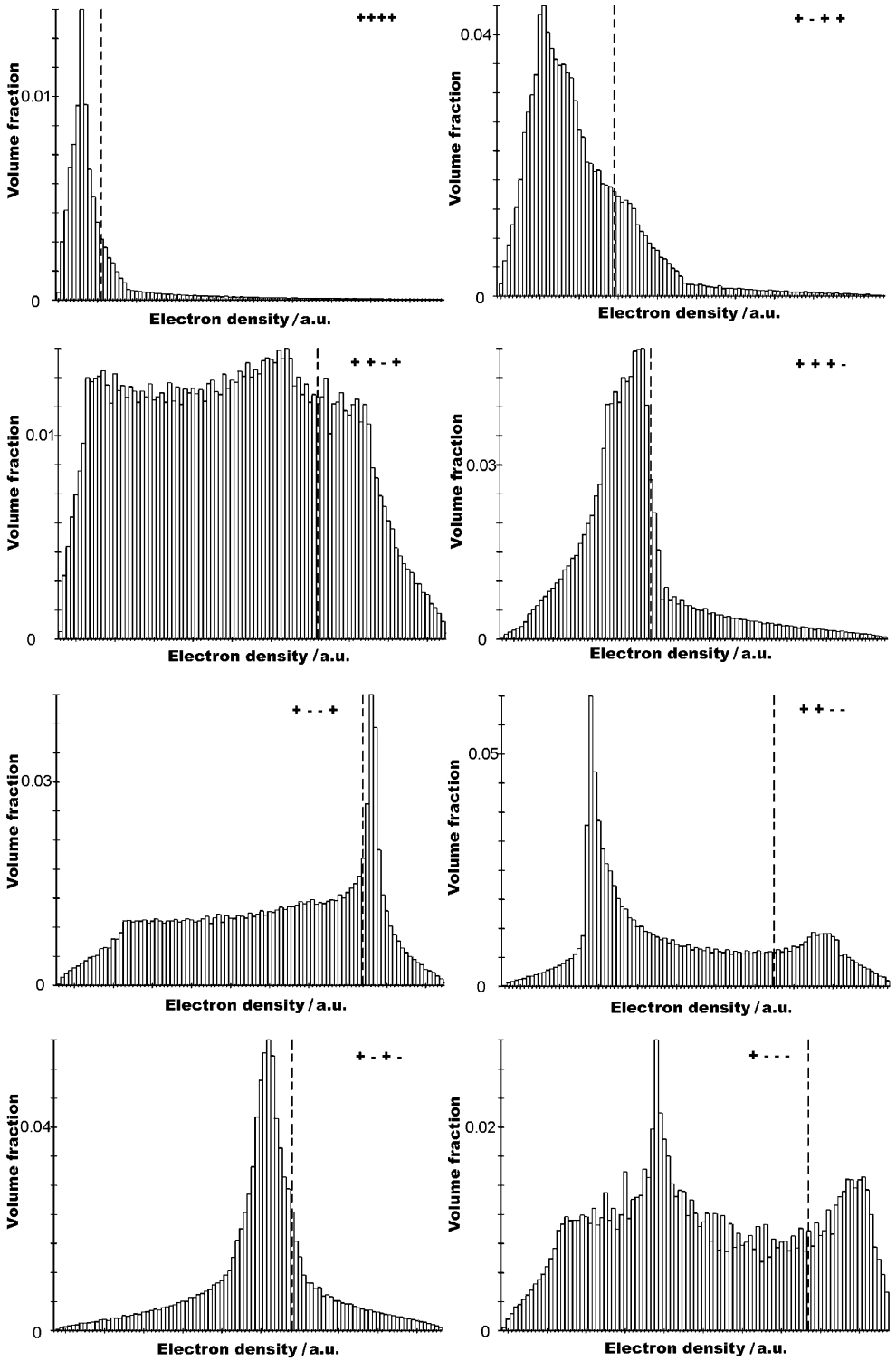

Figure 6. Electron density histograms for eight phase combinations using measured structure factors for X-ray reflections 110, 200, 211 and 220 (see Table 2).

0947-6539/01/0719-4138 $ 17.50+.50/0 *Chem. Eur. J.* **2001**, *7*, No. 19

(marked "++++") shows a remarkably narrow low-density peak. Moreover, the demarcation line separating the 77.5% low-density volume fraction (dashed in Figure 6) is located near the high-density edge of the peak, giving credence to this particular phase choice. The $+\,-{+}{+}$ and $+\,{+}{+}-$ histograms have similar characteristics, but the low electron density peak is significantly broader. The attraction of the $+\,{+}-\,-$ combination is that the histogram shows two discrete peaks with the demarcation line between them. However, the low-density peak is significantly broadened. Other phase choices are not consistent with the condition of microphase separation.

Electron density distributions for phase combinations $+\,{+}{+}{+}$, $+\,-{+}{+}$ and $+\,{+}{+}-$ are all dominated by strong maxima at the vertices (0,0,0) and in the center (½, ½, ½) of the unit cell. EDM of the $z=0$ and $z=0.5$ levels, that is cuts through the base and the center of the unit cell, are shown as surface plots in Figure 7 for the $+\,{+}{+}{+}$ phase combination. The maxima stand out from the comparatively flat background. Equivalent maps for the $+\,-{+}{+}$ and $+\,{+}{+}-$ combinations are similar but with a more uneven background. If the low-density background is identified with liquid-like paraffin chains, a reasonably even density is expected and we therefore favor the $+\,{+}{+}$ phase combination. In the case of the $+\,{+}-\,-$ combination rather unusual electron density distribution is obtained, with maxima surrounding the 0,0,0 and ½,½,½ positions but with minima at these actual special positions. Considering the unusual nature of such a distribution and the general unevenness of ρ this combination is thought unlikely.

The contour plot of the $z=0.5$ level of the most plausible structure, that is $+\,{+}{+}{+}$, is shown in Figure 8. The contours of the central density maximum are nearly circular. In agreement with this and the data for other values of z, the three-dimensional shape of the electron density maxima are very close to spherical. In other words, the aromatic–aliphatic interface is spherical. Hence the structure can be described as consisting of spherical aggregates containing the polymer backbone and the benzyl groups, with the aliphatic chains filling the remaining space.

Various types of simple micellar cubic mesophases have been identified in both thermotropic and lyotropic systems. In surfactant systems, at high surfactant concentration, it was generally accepted that the stability of the cubic mesophases appeared to increase in the following order: SC, FCC, BCC, and $Pm\bar{3}n$.[12–14] Therefore, observation of a BCC phase here in a thermotropic material having similar chemical structure is unusual. As discussed before,[1d, 6] the symmetry selection is influenced by the degree and anisotropy of the distortion of micelles packed in the lattice. According to XRD analysis,[5] and geometrical analysis,[15] of the $Pm\bar{3}n$ structure, the micelles are oblate and significantly distorted. In comparison to $Pm\bar{3}n$, both the anisotropy and the degree of micelle distortion are less in the BCC structure. Indeed, in *BCC* the anisotropy is *zero*. The degree of distortion is inversely related to the hard sphere packing fraction of the lattice. The hard sphere packing fraction is equal to 0.524 for $Pm\bar{3}n$ and 0.680 for BCC. Therefore the micelles of BCC are more spherical. This shape suggests that the interface between the aromatic micelle core and the aliphatic corona is less crowded, as a result of the increased volume fraction of the corona (i.e., three tails per monomer repeat instead of two). Extrapolating, we suspect that, by analogy with other experiments with block copolymers,[16] addition of small amounts of a molecule that solvates the corona is likely to produce even more spherical micelles and result in FCC packing.

Conclusion

A poly(ethyleneimine) with tapered tri(dodecyloxy) benzoyl side groups (i.e., minidendritic side groups),[3] {**poly[(3,4,5)12G1-Oxz]**} with degree of polymerization DP = 20 displays a body-centered cubic (BCC) phase. ED, EDM and TEM imaging confirm definitely the $Im\bar{3}m$ (Q^{229}) space group suggested previously[5] by DSC, TOPM and XRD experiments. Also, the lattice parameter determined by ED, $a=42.4$ Å, is in agreement with $a=42.6$ Å determined by XRD. Furthermore, EDM of the XRD results indicate that **poly[(3,4,5)12G1-Oxz]** self-assembles in a spherical supramolecular minidendrimer. The combined analysis by DSC, TOPM, XRD, ED, TEM and EDM indicated that the supramolecular object contains the polyethyleneimine backbone enclosed in an aromatic core that is microsegregated from the melted *n*-alkyl groups. The self-organization of the supramolecular miniden-

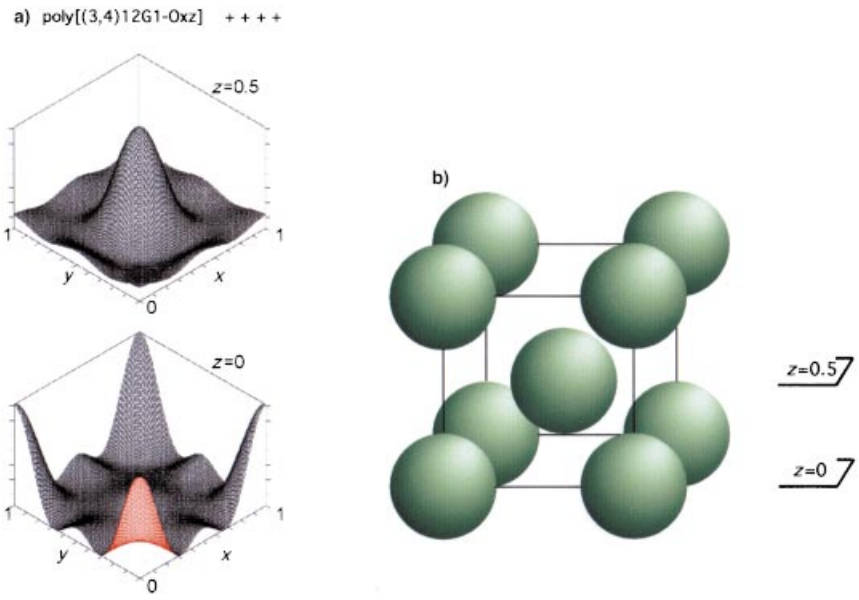

Figure 7. Electron density maps (surface plots) of **poly[(3,4,5)12G1-Oxz]** DP = 20 for $z=0$ and $z=0.5$ sections a) through the $Im\bar{3}m$ cubic unit cell, b) obtained for the phase combination $+\,{+}{+}{+}$.

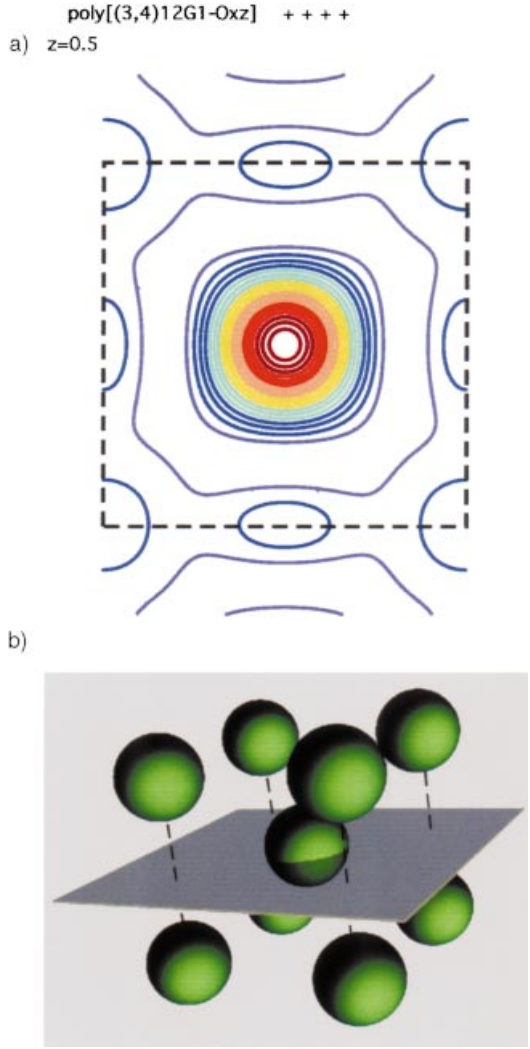

Figure 8. Contour map showing electron density section through the center ($z = 0.5$) of the $Im\bar{3}m$ unit cell. One and a half cells are shown, the broken line delineating one unit cell. Dark blue colour indicates the lowest, and brown colour the highest density. The strong maximum in the center arises from the aromatic region of the micelle situated at the body center (½, ½, ½). The circular contours show that this region has a nearly spherical shape; b) Sketch of the unit cell showing the $z = 0.5$ plane containing the spherical micellar shape shown in a). The edges of the unit cell are marked with dashed lines.

drimer yields an "inverse micellar-like" structure, with the aromatic core concentrated in the corners and in the center of the cubic unit cell and the *n*-alkyl groups radiating out to form a space-filling continuum in the $Im\bar{3}m$ cubic lattice. This manuscript is only the second example of complete structural analysis of a lattice generated from supramolecular dendritic objects and complements the previous example reported from our laboratory on the $Im\bar{3}m$ lattice.[1d, 4]

Experimental Section

The synthesis and XRD analysis of the bulk phase of poly{*N*-[3,4,5-tris-(*n*-dodecan-l-yloxy)benzoyl]ethyleneimine} {**poly[(3,4,5)12G1-Oxz]**} oligomer with DP = 20 (Figure 1) used in this study was previously described.[5] The degree of polymerization (DP) was controlled by the monomer to initiator molar ratio DP = 20 since the polymer was generated by a living cationic ring-opening polymerization reaction. Confirmation of the number-average molecular weight was provided by nuclear magnetic resonance spectroscopic end group analysis and the narrow molecular weight polydispersity ($M_w/M_n = 1.1$) was demonstrated by size-exclusion chromatography.

Phase characterization was undertaken by using a combination of differential scanning calorimetry (DSC), thermal optical polarized microscopy (TOPM) and transmission electron microscopy (TEM). An Olympus BX60 polarizing optical microscope was used in transmission mode, and a Zeiss polarizing microscope used in reflectance. Sample temperature was controlled during optical microscopic examination using a Mettler M80 hot stage.

TEM experiments were conducted on a JEOL JEM-100CX electron microscope operated at 100 kV. A thin film was cast from a 1 % solution in toluene onto carbon-coated mica. To prevent dewetting of the sample during heat treatment, another layer of carbon (much less than 100 nm in thickness) was evaporated on top of the material. The sample was then floated on water and retrieved onto copper grids. Samples were heat treated by first heating up to 130 °C (i.e., isotropic). They were then cooled to 70 °C at a rate of 1 °C min^{-1} and annealed at this temperature for approximately 2 h. Finally, the samples were quenched in liquid nitrogen and examined without staining by TEM. Staining was not used because it was found (by ED) to destroy the structure.

A sample holder capable of rotating the copper grid was used so that the direction of the goniometer tilt axis could be adjusted to coincide with special symmetry axes observed in the sample. Diffraction patterns from the [001], [110], and [111] type zone axes were recorded by using Fuji film FDP UR-V image plates. These image plates have a remarkable dynamic range (covering more than four orders of magnitude in electron dose, that is from 1×10^{-14} to 4×10^{-9} C cm^{-2} at 100 kV) and are able to record very strong and weak reflections simultaneously. This compares very favorably to the dynamic range of the film, which is approximately a factor of 30. The particular limits of sensitivity of the film depend on film type and developing conditions. Typical values are approximately from 1×10^{-11} to 3×10^{-10} C cm^{-2}. The image plates are also useful for quantitative analysis of diffraction intensities and of electron dose.

Due to the high sensitivity of the ordered structure, electron images, and diffraction patterns were recorded using a minimal electron dose. The endpoint dose for the (110) reflection was measured to be approximately 0.014 C cm^{-2} (where now the area represents the area on the specimen itself, not the area on the recording medium, as discussed in the previous paragraph). The value of the endpoint dose is approximately three times greater than the critical dose for polyethylene, which has a similar melting temperature.[17] It is reasonable that the 3-D order of this lattice should be more tolerant to rearrangements produced by the electron beam, because of its greater inherent disorder in comparison to more ordered 3-D crystals. The dose used to obtain lattice images was kept below the critical dose, as confirmed by observation of the (110) electron diffraction (ED) spots after the lattice image was recorded. The image plates were not used for lattice imaging, because wide dynamic range is not required during imaging and because the minimum pixel size (25 μm) of the image plates is larger than the minimum feature size recorded by type SO-163 film.

X-ray diffraction (XRD) patterns were recorded using low-angle cameras at Sheffield University and at the Synchrotron Radiation Source at Daresbury, U.K. The Sheffield camera was equipped with a 18 cm Mar image plate detector/scanner, while a multiwire proportional area detector was used at Daresbury. Absence of preferred orientation was ascertained and intensities were radially integrated and normalized to a line scan format $I(\theta)$. Integrated peak intensities $I_{hkl} = \int I(\theta) d\theta$ are listed in Table 2 for the four most intense peaks. Structure factors F_{hkl}, obtained from Lorentz and multiplicity-corrected intensities, are also listed in Table 2.

Acknowledgement

Financial support by the National Science Foundation, USA DMR-9806684 to S. Hudson and DMR-9996288 and DMR-0102459 to V. Percec are gratefully acknowledged. G. Ungar thanks the Engineering and Physical Science Research Council and acknowledges Dr. B.U. Komanschek of Daresbury Laboratory, UK, for help with the synchrotron experiments.

0947-6539/01/0719-4140 $ 17.50+.50/0

[1] For selected references on cylindrical supramolecular dendrimers self-organized in hexagonal columnar LC lattices reported from our laboratory see: a) V. Percec, G. Johansson, J. Heck, G. Ungar, S. V. Batty, *J. Chem. Soc. Perkin Trans. 1* **1993**, 1411; b) G. Johansson, V. Percec, G. Ungar, D. Abramic, *J. Chem. Soc. Perkin Trans. 1* **1994**, *447*; c) V. Percec, G. Johansson, G. Ungar, J. Zhou, *J. Am. Chem. Soc.* **1996**, *118*, 9855; d) S. D. Hudson, H.-T. Jung, V. Percec, W.-D. Cho, G. Johansson, G. Ungar, V. S. K. Balagurusamy, *Science* **1997**, *278*, 449; e) V. Percec, W.-D. Cho, P. E. Mosier, G. Ungar, D. J. P. Yeardley, *J. Am. Chem. Soc.* **1998**, *120*, 11061. For examples of cylindrical supramolecular dendrimers self-organized in a hexagonal columnar LC lattice reported from other laboratories see: f) U. Stebani, G. Lattermann, *Adv. Mat.* **1995**, *7*, 578; g) D. Pesak, J. S. Moore, *Angew. Chem.* **1997**, *109*, 1709; *Angew. Chem. Int. Ed. Engl.* **1997**, *36*, 1636; h) M. Suarez, J.-M. Lehn, S. C. Zimmerman, A. Skoulios, B. Heinrich, *J. Am. Chem. Soc.* **1998**, *120*, 9526; i) H. Meier, M. Lehmann, U. Kolb, *Angew. Chem.* **1998**, *110*, 666; *Angew. Chem. Int. Ed.* **1998**, *37*, 643; j) M. Lehmann, B. Schartel, M. Hennecke, H. Meier, *Tetrahedron* **1999**, *55*, 13377; k) H. Meier, M. Lehmann, U. Kolb, *Chem. Eur. J.* **2000**, *6*, 2462; l) M. Brewis, G. J. Clarkson, A. M. Holder, N. B. McKeon, *Chem. Commun.* **1998**, 969; m) M. Brewis, G. J. Clarkson, V. Goddard, M. Helliwell, A. M. Holder, N. B. McKeown, *Angew. Chem.* **1998**, *110*, 1185; *Angew. Chem. Int. Ed.* **1998**, *37*, 1092; n) M. Brewis, G. J. Clarkson, M. Helliwell, A. M. Holder, N. B. McKeown, *Chem. Eur. J.* **2000**, *6*, 4630; for other 2-D lattices from dendritic building blocks see: o) V. Percec, P. Chu, G. Ungar, J. Zhou, *J. Am. Chem. Soc.* **1995**, *117*, 11441.

[2] For selected references on cylindrical macromolecular dendrimers self-organized in hexagonal columnar LC lattices see: a) V. Percec, J. Heck, M. Lee, G. Ungar, A. Castillo, *J. Mater. Chem.* **1992**, *2*, 1033; b) V. Percec, J. Heck, D. Tomazos, F. Falkenberg, H. Blackwell, G. Ungar, *J. Chem. Soc. Perkin Trans. 1* **1993**, 2799; c) V. Percec, J. Heck, D. Tomazos, G. Ungar, *J. Chem. Soc. Perkin Trans. 2* **1993**, 2381; d) V. Percec, D. Tomazos, J. Heck, H. Blackwell, G. Ungar, *J. Chem. Soc. Perkin Trans. 2* **1994**, 31; e) V. Percec, D. Schlueter, Y. K. Kwon, J. Blackwell, M. Möller, P. J. Slangen, *Macromolecules* **1995**, *28*, 8807; f) G. Johansson, V. Percec, G. Ungar, J. P. Zhou, *Macromolecules* **1996**, *29*, 646; g) V. Percec, D. Schlueter, J. C. Ronda, G. Johansson, G. Ungar, J. P. Zhou, *Macromolecules* **1996**, *29*, 1464; h) V. Percec, D. Schlueter, *Macromolecules* **1997**, *30*, 5783; i) V. Percec, C.-H. Ahn, W.-D. Cho, A. M. Jamieson, J. Kim, T. Leman, M. Schmidt, M. Gerle, M. Möller, S. A. Prokhorova, S. S. Sheiko, S. Z. D. Cheng, A. Zhang, G. Ungar, D. J. P. Yeardley, *J. Am. Chem. Soc.* **1998**, *120*, 8619; j) S. A. Prokhorova, S. S. Sheiko, M. Möller, C.-H. Ahn, V. Percec, *Macromol. Rapid Commun.* **1998**, *19*, 359; k) V. Percec, D. Schlueter, G. Ungar, S. Z. D. Cheng, A. Zhang, *Macromolecules* **1998**, *31*, 1745; l) S. A. Prokhorova, S. S. Sheiko, C.-H. Ahn, V. Percec, M. Möller, *Macromolecules* **1999**, *32*, 2653; m) V. Percec, C.-H. Ahn, G. Ungar, D. J. P. Yeardley, M. Möller, S. S. Sheiko, *Nature* **1998**, *391*, 161; n) V. Percec, M. N. Holerca, *Biomacromolecules* **2000**, *1*, 6; o) S. A. Prokhorova, S. S. Sheiko, A. Mourran, R. Azumi, U. Beginn, G. Zipp, C.-H. Ahn, M. N. Holerca, V. Percec, M. Möller, *Langmuir* **2000**, *16*, 6862.

[3] For the co-assembly of a hexagonal columnar LC superlattice and the demonstration of the synthetic capabilities of minidendritic building blocks see: V. Percec, C.-H. Ahn, T. K. Bera, G. Ungar, D. J. P. Yeardley, *Chem. Eur. J.* **1999**, *5*, 1070.

[4] For the first example of spherical supramolecular dendrimers self-organized in a $Pm\bar{3}n$ cubic LC lattice and a detailed analysis by XRD and electron density maps see: V. S. K. Balagurusamy, G. Ungar, V. Percec, G. Johansson, *J. Am. Chem. Soc.* **1997**, *119*, 1539.

[5] D. J. P. Yeardley, G. Ungar, V. Percec, M. N. Holerca, G. Johansson, *J. Am. Chem. Soc.* **2000**, *122*, 1684.

[6] S. D. Hudson, H.-T. Jung, P. Kewsuwan, V. Percec, W.-D. Cho, *Liq. Cryst.* **1999**, *26*, 1493.

[7] For examples of spherical supramolecular dendrimers self-organized in a $Pm\bar{3}n$ lattice; a) V. Percec, W.-D. Cho, G. Ungar, *J. Am. Chem. Soc.* **2000**, *122*, 10273; b) V. Percec, W.-D. Cho, G. Ungar, D. J. P. Yeardley, *Angew. Chem.* **2000**, *112*, 1661; *Angew. Chem. Int. Ed.* **2000**, *39*, 1597; c) V. Percec, W.-D. Cho, G. Ungar, D. J. P. Yeardley, *J. Am. Chem. Soc.* **2001**, *123*, 1302.

[8] For several representative publications on complex phase behavior in block copolymers see for example: a) F. S. Bates, *Science* **1991**, *251–254*, 898; b) M. A. Hillmyer, F. S. Bates, K. Almdal, K. Mortensen, A. J. Ryan, J. P. A. Fairclough, *Science* **1996**, *271*, 976; c) G. H. Fredrikson, F. S. Bates, *Annu. Rev. Mater. Sci.* **1996**, *26*, 501; d) E. L. Thomas, D. M. Anderson, C. S. Henkee, D. Hoffman, *Nature* **1988**, *334*, 598; e) T. A. Shefelbine, M. E. Vigild, M. W. Matsen, D. A. Hajduk, M. A. Hillmyer, E. L. Cussler, F. S. Bates, *J. Am. Chem. Soc.* **1999**, *121*, 8457.

[9] E. Pedemonte, A. Turturro, U. Bianchi, P. Devetta, *Polymer* **1973**, *14*, 145.

[10] F. S. Bates, R. E. Cohen, C. V. Berney, *Macromolecules* **1982**, *15*, 589.

[11] a) Y. K. Kwon, S. Chvalun, J. Blackwell, V. Percec, J. Heck, *Macromolecules* **1995**, *28*, 1552; b) G. Ungar, V. Percec, M. N. Holerca, G. Johansson, J. A. Heck, *Chem. Eur. J.* **2000**, *6*, 1258.

[12] R. G. Larson, *Chem. Eng. Sci.* **1994**, *49*, 2833.

[13] P. Sakya, J. M. Seddon, R. H. Templer, R. J. Mirkin, G. J. T. Tiddy, *Langmuir* **1997**, *13*, 3706.

[14] P. Ziherl, R. D. Kamien, *Phys. Rev. Lett.* **2000**, *85*, 3528.

[15] J. Charvolin, J. F. Sadoc, *J. Phys. France* **1988**, *49*, 521.

[16] a) G. A. McConnell, A. P. Gast, J. S. Huang, S. D. Smith, *Phys. Rev. Lett.* **1993**, *71*, 2102; b) G. A. McConnell, A. P. Gast, *Phys. Rev. E* **1996**, *54*, 5447; c) G. A. McConnell, A. P. Gast, *Macromolecules* **1997**, *30*, 435.

[17] S. Kumar, W. W. Adams, *Polymer* **1990**, *31*, 15.

Received: February 1, 2001 [F3047]